

---

---

# The peripheral nerves: update on ultrasound and magnetic resonance imaging

---

---

I. Möller<sup>1</sup>, M. Miguel<sup>2</sup>, D.A. Bong<sup>1</sup>, F. Zaottini<sup>3</sup>, C. Martinoli<sup>4</sup>

---

---

<sup>1</sup>Instituto Poal de Reumatologia, University of Barcelona, Spain, and EULAR Working Group Anatomy for the Image;

<sup>2</sup>Department of Pathology and Experimental Therapeutics, Human Anatomy and Embryology Unit, University of Barcelona, Spain;

<sup>3</sup>Department of Health Sciences, DISSAL, University of Genoa;

<sup>4</sup>Department of Health Science, University of Genoa, Ospedale Policlinico San Martino, Genoa, Italy.

Ingrid Möller, MD

Maribel Miguel, MD

David A. Bong, MD

Federico Zaottini, MD

Carlo Martinoli, MD

Please address correspondence to:

Dr David A. Bong,

Instituto Poal de Reumatologia,

Calle Castanyer 15,

08022 Barcelona, Spain.

E-mail: dabong47@gmail.com

Received on September 11, 2018;

accepted on September 13, 2018.

*Clin Exp Rheumatol* 2018; 36 (Suppl. 114): S145-158.

© Copyright CLINICAL AND

EXPERIMENTAL RHEUMATOLOGY 2018.

**Key words:** peripheral nervous system, anatomy, image, magnetic resonance, high-resolution ultrasound

## ABSTRACT

*The motor and sensory branches of the somatic peripheral nervous system (PNS) can be visualised by different imaging systems. This article focuses on imaging of peripheral nerves by magnetic resonance imaging (MRI) and high-resolution ultrasound (US). The anatomic basis of the peripheral nerve image, common pathologies and clinical value of US and MRI imaging of peripheral nerves are reviewed.*

## Introduction

Nerve pathology may be a cause of chronic pain and disability. The initial diagnostic evaluation of the peripheral nervous system (PNS) involves a thorough patient history and physical examination. Neurophysiologic testing is often required owing to the difficulties in precisely assessing the degree of nerve damage and to differentiate between demyelination and axonal degeneration. These tests measure electrical activity of nerves according to different parameters, such as latency, amplitude and conduction velocity (1). The accuracy of nerve conduction studies may, however, be influenced by a variety of factors, including age, gender, height and body mass index (2, 3).

The relatively recent application of imaging techniques, such as ultrasound (US) and magnetic resonance (MR) imaging, have allowed detailed visualisation of the peripheral nervous system providing information concerning morphological alteration of the nerve and surrounding tissues (4, 5). Imaging also may be used to assess the status of innervated musculature that aid in underlying diagnosis, localisation of disease and recognition of the degree of nerve damage. In addition, it can be very useful in monitoring of response to therapy and prognosis for recovery. US has some advantages over MR, including its availability and that it permits higher resolution dynamic real-time imaging

of the nerve along its trajectory along with immediate one-to-one comparison with the contralateral structures (6, 7). In addition, US-guidance has led to the development of a variety of interventional procedures. The use of US is becoming widespread in providing accurate and safe regional anesthesia as well as focal and regional pain management. It has also becoming an increasingly important component of musculoskeletal specialties such as physical medicine and rehabilitation and sports medicine.

## Anatomical considerations

The PNS includes spinal nerves that originate from the combination of dorsal and ventral roots of the spinal cord and the cranial nerves originating from the forebrain and brain stem. The dorsal roots of spinal nerves encompass sensory axons, whereas the ventral roots contain motor axons. Soon after crossing the intervertebral foramina, spinal nerves split into a delicate posterior (dorsal) ramus innervating muscles and skin of the back and a large anterior (ventral) ramus innervating limb muscles and the skin of the anterior aspect of the body. Both rami are hybrids as they contain sensory and motor fibres. Cranial nerves may be sensory or motor. Nerve fibres (axons) are surrounded by a myelin sheath or non-myelinated, such as in the case of the smaller sensory nerves. Groups of axons are bundled together and embedded in a delicate connective tissue, the endoneurium (Fig. 1). Each bundle of endoneurium-embedded axons is then surrounded by a distinct membrane, the perineurium, to form a fascicle.

In larger nerves, the perineurium acts as a “blood-nerve barrier” and is in continuity with the pia-arachnoid of the meninges being formed by layers of flat cells in a matrix of collagen fibres that are arranged concentrically around single nerve fascicles (8). The perineu-

Competing interests: none declared.

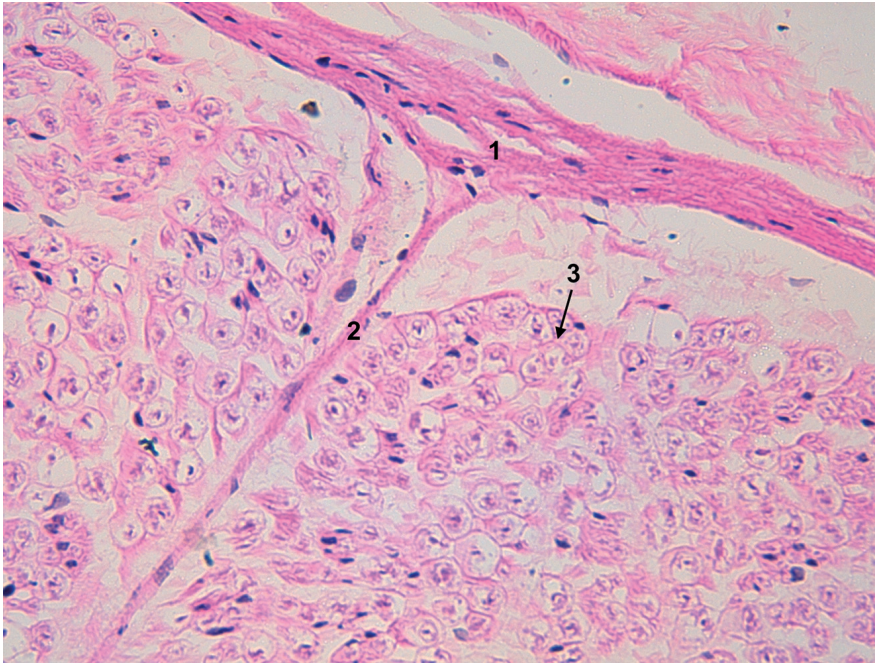


**Fig. 1.** Microscopic section of peripheral nerve demonstrating the endoneurium (1), perineurium (2) and epineurium (3).

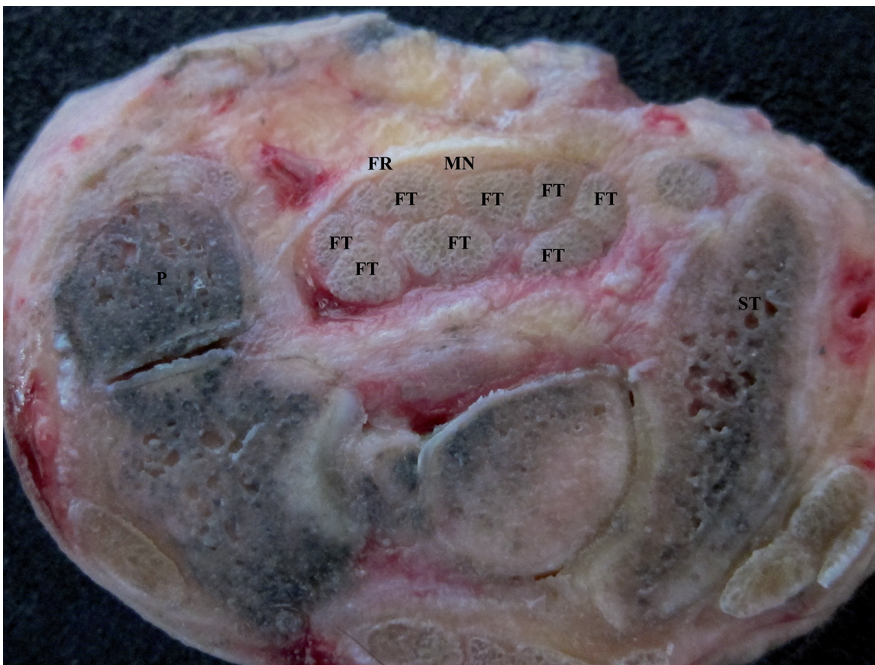


**Fig. 2.** Carpal tunnel. Axial section through the carpal tunnel at the wrist. Note the median nerve (MN) in the tunnel which is formed by the overlying flexor retinaculum (FR) which connects the pisiform (P) to the scaphoid tubercle (ST) of the carpus. The flexor tendons (FT) of the thumb and fingers are also in the tunnel.

rium helps to regulate and, also, protect the axons from tensile and compressive stresses.

Fascicles may travel directly and independently within the nerve as individual “cords” or “cables” as the median nerve does in the distal arm or may interconnect with other fascicles forming

a plexus, as observed frequently in the median nerve at the antecubital fossa (9). Nerve fascicles are then bound together by a tough outer epineurium made up of loose connective tissue to form a typical peripheral nerve (10). The space between the outer epineurium and the perineurium surrounding

the fascicles is referred to as the interfascicular epineurium. The amount of interfascicular epineurium is related directly to the number of fascicles and is more abundant in areas requiring greater mobility, such as where nerves cross joints. On the external side, the outer epineurium forms a continuum with surrounding loose areolar connective tissue, the so-called mesoneurium. Nerves are vascularised throughout their entire trajectory and also contain a lymphatic network. The mesoneurium contains a complex system of perineural vessels, the so-called “vasa nervorum”, and guarantees some nerve mobility while protecting the microvascular architecture. Perineural vessels give off penetrating branches that enter the nerve bundle and run parallel to the fascicles, embedded in the interfascicular epineurium. Along the perivascular plexuses, small nerve endings, the “nerve-nervorum”, provide sympathetic innervation to the nerve bundles.

Familiarity with nerve trajectory and anatomic passageways is critical for a successful evaluation with high-resolution US and MR imaging. Nerve localisation, recognition of anatomical variants and detailed knowledge of the areas in which entrapment is most likely to occur enhance the accuracy of imaging evaluation. Knowledge of specific anatomic structures (“landmarks”) or reference points is essential in localising and assessing peripheral nerves:

1. nerves pass through narrow anatomic passageways in the limbs, the so called osteofibrous tunnels, that typically are delimited by a bony floor and retinacular roof (*e.g.* the carpal tunnel, where the median nerve may be entrapped) (Fig. 2);
2. nerves often are accompanied by satellite vessels or guardian muscles for long segments of their course (*e.g.* the anterior interosseous nerve accompanied by the anterior interosseous artery as it travels down through the forearm; the ulnar nerve covered by the flexor carpi ulnaris muscle) (Fig. 3);
3. nerves may cross fascial sheets that overlie muscles or separate compartments at specific locations (*e.g.* the sensory branch of the radial nerve



**Fig. 3.** Anterior interosseous nerve. Deep topographical dissection of the anterior (volar) forearm showing the anterior interosseous nerve (yellow markers) traveling jointly with the anterior interosseous artery (red markers) on the surface of the interosseous membrane from the antecubital fossa (right) to the wrist (left).

piercing the fascia of the distal forearm after leaving the undersurface of the brachioradialis; the superficial peroneal nerve as it penetrates the lower leg fascia 10 cm above the lateral malleolus (Fig. 4).

An in-depth knowledge of soft-tissue anatomy may help in nerve identification and often clarifies the aetiology and pathophysiology of some nerve diseases.

### Ultrasound and MR imaging of peripheral nerves

#### Ultrasound imaging

Peripheral nerves and perineural structures can be examined using US and MR imaging on their long-axis and short-axis but owing to their serpentine course, the short-axis usually is superior to the long-axis (11, 12). On short-axis images, nerves exhibit a rounded, ovoid or somewhat flattened shape containing multiple individualised hypoechoic/anechoic dots (each “dot” representing a fascicle) giving rise to a “honeycomb” appearance (13). This appearance is similar to the presence of “poppy seeds within a muffin” (Fig. 5A). On long-axis images, nerves show narrow, elongated structures with a fascicular appearance due to alternating hypoechoic and hyperechoic bands (Fig. 5B). The hypoechoic/anechoic dots represent the fascicles (including the perineurium). They are surrounded by a hyperechoic background related to the interfascicular and, on the external side, to the outer epineurium.

At the level of osteofibrous tunnels, the outer epineurium may occasionally ap-

pear more hyperechoic relative to the surrounding perineural fat. This feature is, however, inconstant and rarely recognised outside tunnels. Unlike absolutely uniform and fibrillar structure of tendons, the fascicular echotexture of nerves does not display the property of anisotropy. The term “anisotropy” essentially refers to a characteristic of a certain structure or substance being directionally dependent. Specifically in US, this represents a dramatic change in ecogenicity (from white “hyperechoic” to dark grey-black “hypoechoic-anechoic” when toggling the probe from side-to-side or up-down thus changing the direction at which the US beam strikes a specific structure and altering the subsequent angle of reflection.

The preferred technique for examination is quite dynamic. The probe, in short axis to the nerve, is slid along the nerve proximal-to-distal or distal-to-proximal while toggling gently from side-to-slide to minimise artifact and noise created by inappropriate orientation of the beam; this scanning technique is commonly referred to as the “elevator” technique. This approach provides a detailed morphologic study of the nerve and perineural structures.

When an appropriate image of the nerve is captured, quantitative measurements, such as the axial diameter or the cross-sectional area (CSA) of the nerve may be taken to better quantify pathologic changes affecting the size of the nerve bundle or individual fascicles. In several nerve disorders, the most relevant morphologic changes affecting nerves include generalised nerve enlargement,

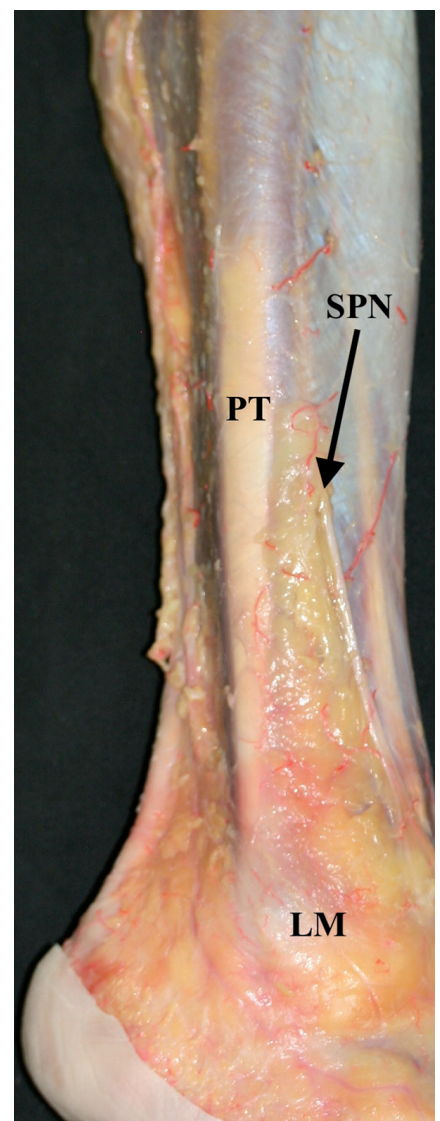
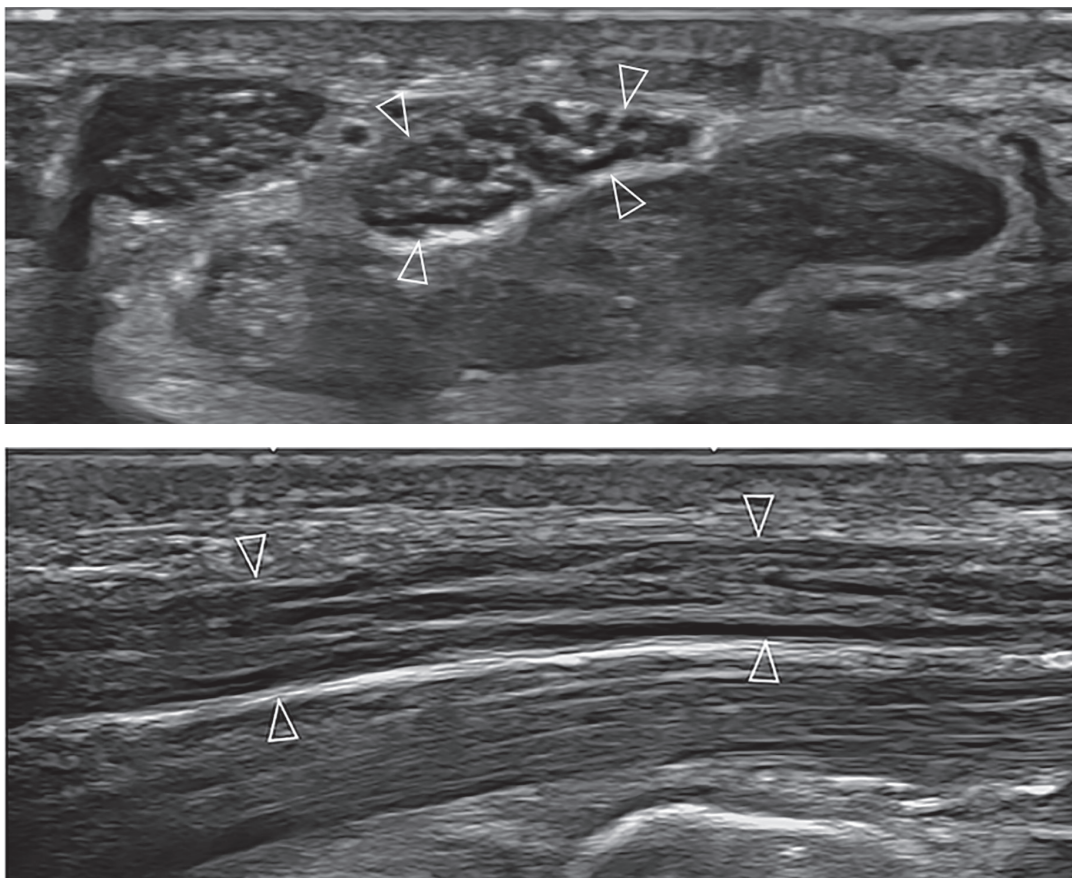


**Fig. 4.** Superficial peroneal nerve. The superficial peroneal nerve (SPN) emerges from the fascia of the lateral leg, a common site of nerve injury with extreme inversion owing to the nerves fixation at this point. LM: lateral malleolus; PT: peroneal tendons.

**Fig. 5.** US appearance of normal nerves.

(A) Short-axis and (B) long-axis 24-8MHz US images of the median nerve at wrist.

**A:** The nerve (arrowheads) is composed of rounded hypoechoic dots (fascicles) embedded in a homogeneous hyperechoic background (epineurium).  
**B:** The nerve (arrowheads) is characterised by multiple hypoechoic parallel linear areas (fascicles) separated by hyperechoic bands (epineurium).



grossly enlarged fascicles, loss of the fascicular pattern, focal changes in the nerve shape and size and intraneural vascularisation noticed at Doppler imaging (14, 15).

#### Magnetic resonance imaging

On MR imaging, the nerve fascicle is also the smallest unit that can be depicted similar to US (16). With MR, fascicles can be identified in large nerves, but not invariably in small distal branches. The use of high matrix, thin slices and small field-of-view usually is required to improve spatial resolution and fascicular depiction. On T1-weighted images, individual nerve fascicles appear hypointense and surrounded by connective tissue that looks hyperintense due to its fat content (Fig. 6A-B). Fat suppression with fast short-tau inversion recovery (STIR) or by frequency-selective saturation of the fat resonance is valuable to improve depiction of intraneural fascicles enhancing contrast resolution (16). Using these sequences, the appearance of nerve fascicles ranges from isoin-

tense to mildly hyperintense, relative to the normal muscle. Nerve fascicles containing more abundant endoneurial fluid may have slightly higher signal intensity than the surrounding connective tissue (16).

Nerves may show reduction of signal intensity when they are oriented at an angle of approximately 55° to the magnetic field using T2-weighted sequences with long TEs, an artifact called “magic angle effect,” similar to tendons (17). Examiners must be aware of this artifact, as it may mimic disease. In normal states, nerves do not show contrast enhancement after gadolinium administration because of the integrity of the blood-nerve barrier (18).

In addition to conventional T1- and T2-weighted sequences, MR neurography is an additional acquisition protocol that is able to offer nerve-selective information with increased depiction of the intraneural fascicular pattern (19-24). This technique requires use of high-resolution phased-array coils and heavily T2-weighted (TE 90ms) turbo spin-echo images with fat and

flow suppression to remove signal from non-neural structures (21, 25). By nulling the signal from the epineurium and nerve surroundings, fascicles become markedly hyperintense on MR neurography (Fig. 7A-B-C). Using MR neurography, the nerve can then be reconstructed using 3D-rendering algorithms. Because nerve bundles have a highly ordered histologic architecture, the directional motion of intraneural water can be measured using diffusion-weighted imaging sequences.

Diffusion tensor imaging is a technique for imaging tissue anisotropy. It uses measurements related to the motion of water molecules in anisotropic media to provide information about orientation and degree of architectural organisation of tissues. Tractography is the mathematical rendering used to provide 3D visualisation of fibre tracts and assessment of the orientation of nerve fibres (26, 27). It includes the mean apparent diffusion coefficient (ADC) and mean fractional anisotropy (FA). Fibre tracking acquisition makes use of a spin-echo single-shot diffusion-weighted

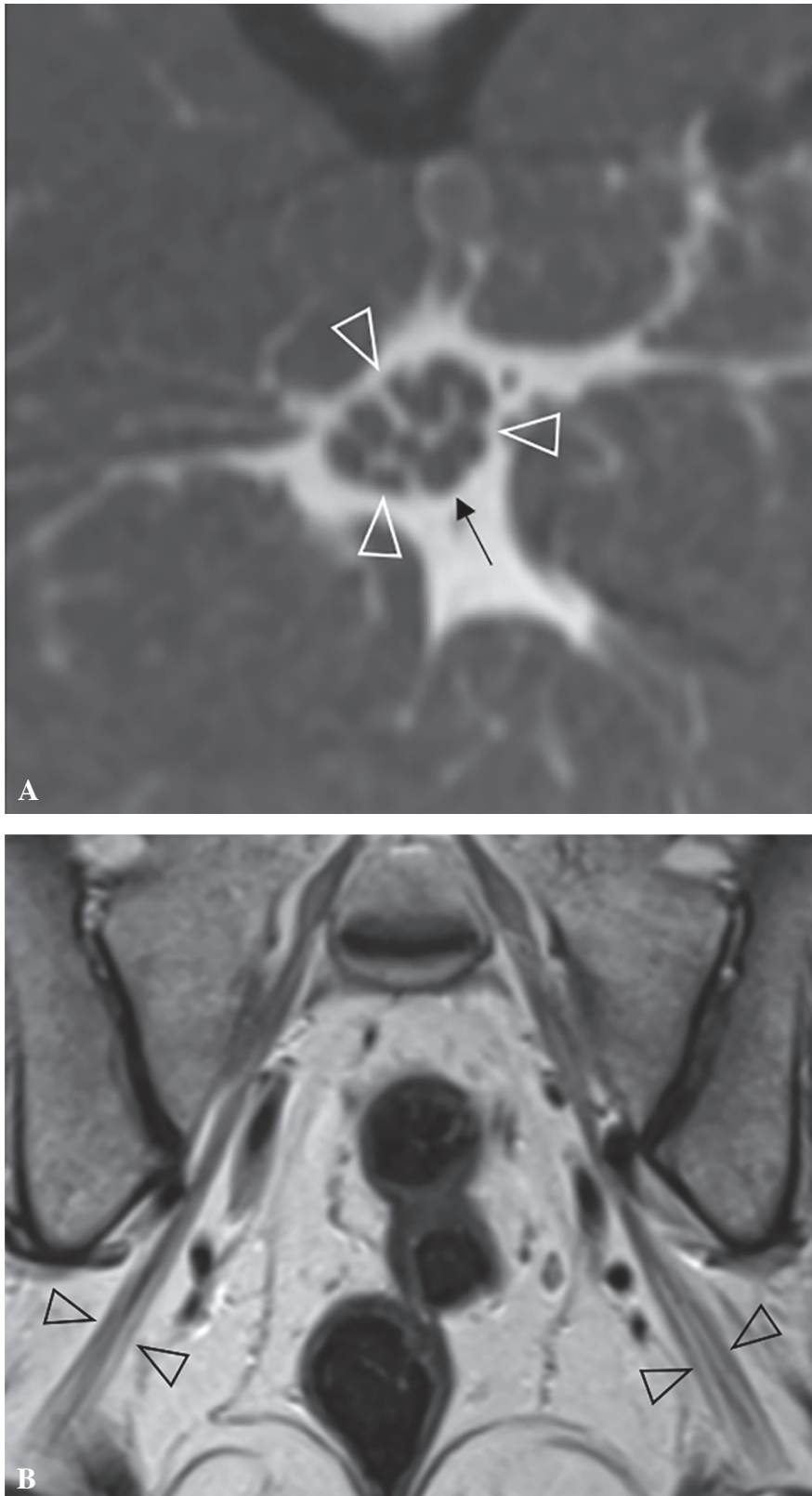


**Fig. 6.** MR imaging of normal nerves.

**A:** Short-axis proton density MR image of the mid-thigh demonstrates the sciatic nerve (arrowheads) made up of hypointense rounded fascicles (arrow) surrounded by hyperintense epineurium. The nerve boundaries look undefined as the signal intensity from outer epineurium does not differ from that of perineural fat.

**B:** Coronal T1-weighted MR image shows the right and left sciatic nerves (arrowheads) descending the pelvis as elongated cords made up of multiple hypointense parallel linear fascicles.

EPI sequence with fat suppression. Colour-coded maps are used to represent the direction of anisotropic structures. With this technique, any pathologic condition affecting the integrity and microscopic architecture of nerve fibres would alter nerve depiction (28-30).

The use of tractography is promising, but is limited to the evaluation of large nerve bundles can be evaluated. Meticulous and extenuating postprocessing is required. At its current state of development, tractography cannot be considered part of the standardised MR imaging protocols to study nerve diseases.

#### *Muscle diseases*

In addition to the assessment of nerves, both US and MR imaging may also reveal muscle changes secondary to the denervation process, as an indirect sign of nerve dysfunction (16, 31). US assessment of denervation relies on detection of volume loss and hyperechoic appearance of the affected muscles. In acute and subacute denervation, MR imaging demonstrates diffusely high signal intensity on fluid-sensitive sequences related to muscle oedema, due to increased intramuscular blood volume and extracellular fluid, and normal signal intensity on T1-weighted images. By contrast, chronically denervated muscles exhibit increased signal intensity on T1-weighted images and substantial loss in bulk of muscles resulting from fatty infiltration and atrophy (31).

US is not as accurate as MR imaging to differentiate early denervation related to accumulation of intramuscular extracellular oedema from fatty atrophy, although, both processes share a similar echotextural appearance. Using diffusion-weighted imaging, denervated muscles may show increased ADC due to early expansion of the extracellular fluid space in these muscles (32).

#### **Entrapment neuropathies**

Entrapment neuropathies usually are the result of chronic or dynamic compression of nerves in fibro-osseous or fibromuscular tunnels. Osteofibrous tunnels have non-extensible walls and a variety of space-occupying lesions, such as accessory muscles, ganglion cysts, bony spurs and synovial pro-

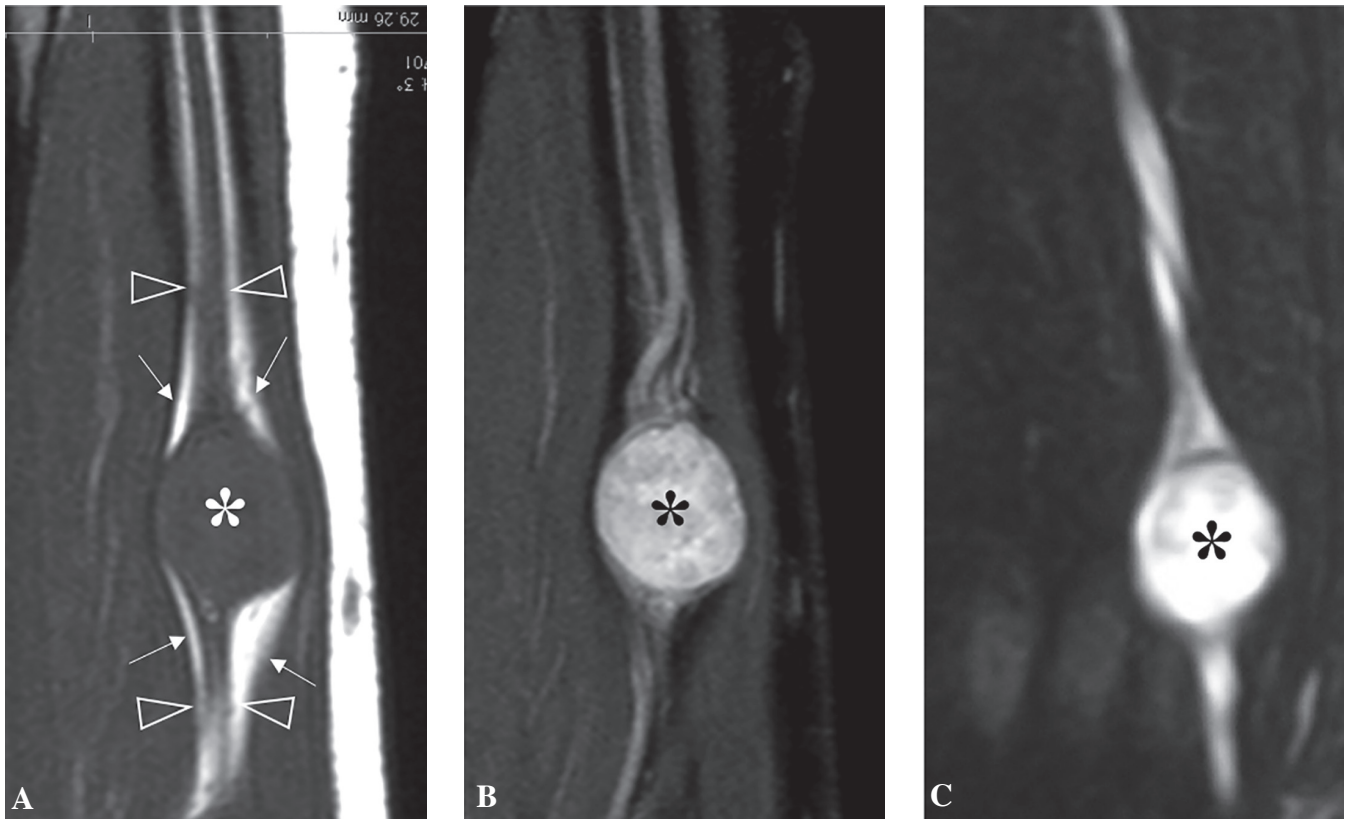


**Fig. 7.** Common MR pulse sequences for nerve imaging.  
**A:** Long-axis T1-weighted MR image of a schwannoma (asterisk) of the ulnar nerve (arrowheads). Both nerve and tumour appear homogeneously isointense to the adjacent muscles. A thin band of intervening hyperintense fat (arrows) is observed between them and the adjacent muscles.  
**B:** Long-axis fat-suppressed T2-weighted MR image shows higher signal intensity of the mass (asterisk) and better contrast resolution with the adjacent soft-tissues.  
**C:** MR neurography provides an angiographic-like image of the nerve and tumour (asterisk) over a black background. This advanced technique gets selective suppression of any signal from muscles, fat and vessels, thus enhancing the conspicuity of nerve tissue signal.

cesses may elevate pressure within them and cause nerve compression. Once established, chronic compression then results in nerve ischaemia, Wallerian degeneration of axons and intraneural fibrosis. Nerve conduction velocity testing may contribute to the diagnosis, but the parameters used are characterised by a high rate of false negatives, cannot identify the cause of nerve entrapment and, in many instances, are unable to identify the exact level of compression along the course of a nerve. US has high spatial resolution and can explore osteofibrous tunnels and their contents using static and dynamic scans (33).

Based on US assessment, nerve compressive syndromes can be grouped into three main classes:

1. Large nerves (*e.g.* median, ulnar, peroneal, tibial) that are easily imaged by US at the compression site using conventional small parts transducers (frequency band up to 13MHz). As-

essment of nerve changes is based on pattern recognition analysis and, at least for the carpal and cubital tunnels, on measurement of the nerve cross-sectional area (CSA). For this class, the diagnostic performance of US can be considered nearly equivalent to MR imaging.

2. Small nerves (*e.g.* posterior and anterior interosseous, musculocutaneous, sural, distal divisional branches of large nerves) of caliber <2mm. The evaluation of these nerves requires high-end equipment and higher frequency probes (frequency band up to 24MHz). The diagnosis relies exclusively on pattern recognition as these nerves are too small for a reliable CSA measurement. There is no objective evidence comparing the performance of US and MR imaging in depicting pathology of these nerves but, in our opinion, US equipped with an appropriate transducer and in experienced hands often seems to be

superior to MR imaging. The main advantage of US compared with MR is its ability to distinguish distal nerves from vessels. In addition, MR imaging cannot rely on detection of muscle denervation changes when evaluating distal branches, as many of these distal nerves branches are purely sensory.

3. Small (*e.g.* inferior calcaneal) or large (*e.g.* femoral and sciatic in their intrapelvic course) nerves that are poorly visible or not accessible at US due to a too deep course or intervening bone. In these instances, MR imaging can be considered the technique of choice to provide adequate characterisation of nerve disease.

Wherever the entrapment site, the main US signs of entrapment neuropathies are pathognomonic. The nerve appears flattened at the site of compression and swollen proximally (Fig. 8A). An abrupt transition (notch sign) is observed between flattened and swollen segments.

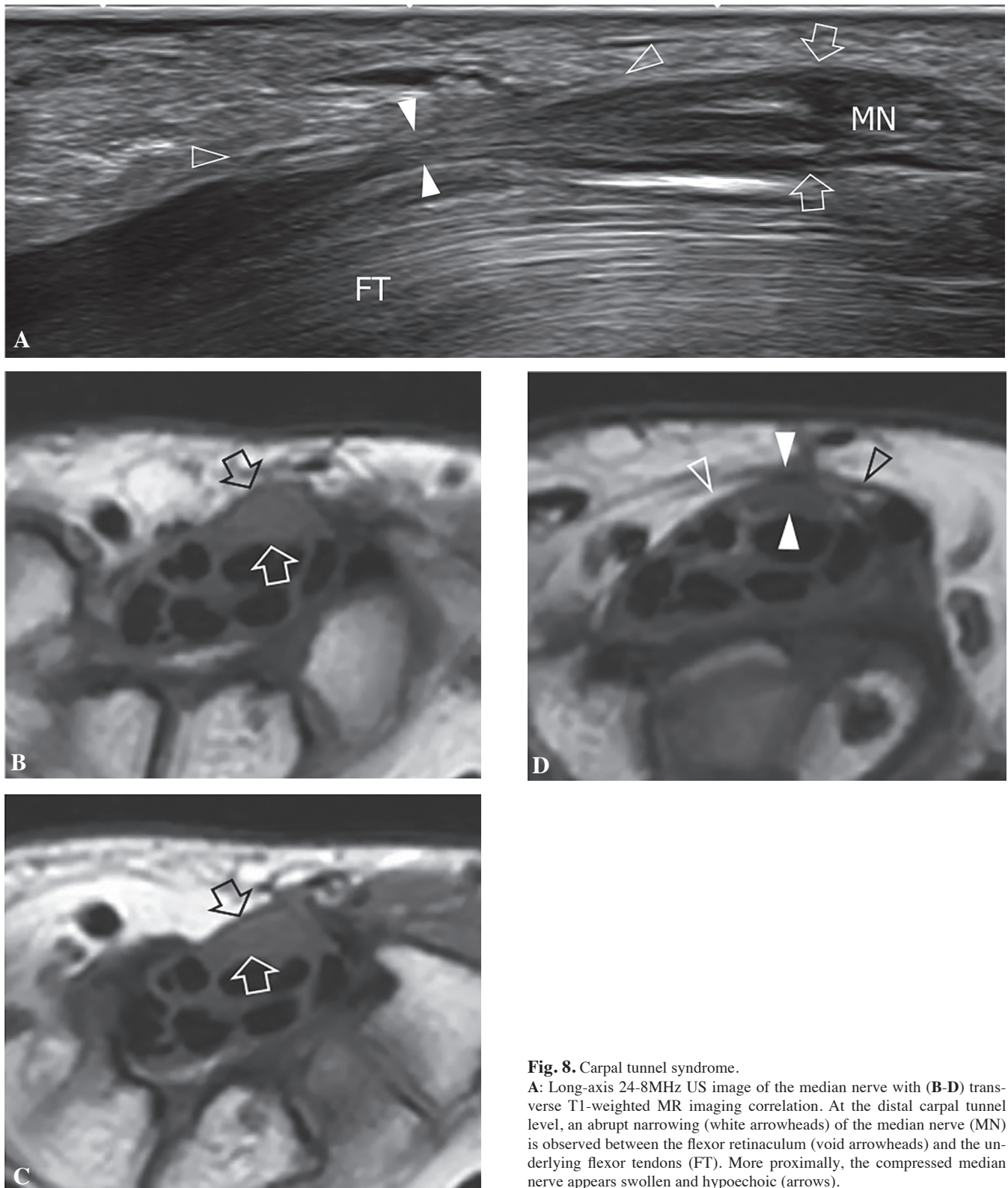


**Fig. 8.** Carpal tunnel syndrome.

**A:** Long-axis 24-8MHz US image of the median nerve with **(B-D)** transverse T1-weighted MR imaging correlation. At the distal carpal tunnel level, an abrupt narrowing (white arrowheads) of the median nerve (MN) is observed between the flexor retinaculum (void arrowheads) and the underlying flexor tendons (FT). More proximally, the compressed median nerve appears swollen and hypoechoic (arrows).

In the early phases of compression, intraneural oedema and venous congestion invariably lead to nerve swelling. The increased water content underlying nerve enlargement has been found to correlate with axon loss (axonotmesis)

and there is a positive relationship between nerve CSA and severity of EMG findings. The nerve echotexture may become uniformly hypoechoic due to swollen fascicles packed together and reduced echogenicity of the epineurium.

These changes are more profound in severe longstanding compression. Occasionally, intraneural hyperaemia can be appreciated at Doppler imaging (34, 35). Similar to US, MR imaging can show nerve enlargement, intraneural oedema,

and gadolinium enhancement as main signs of entrapment neuropathy (36, 37). In addition, it can reveal downstream effects such as denervation changes in muscle (38-40).

Although specific sequence protocols have not been standardised yet for compressive neuropathies, the acquisition protocol usually includes both T1-weighted (to demonstrate anatomy) and fluid-sensitive sequences (manifesting intraneural oedema and characterisation of any mass lesions) (Fig. 8B-D). Acute axonal nerve lesions are depicted by high signal intensity on T2-weighted and STIR sequences and increased nerve size (41). Intravenous contrast administration may be used for distinguishing between cystic and soft-tissue mass lesions and outlining vascular anatomy (42).

Many inconsistencies are seen in literature concerning entrapment syndromes in nerve measurements related cut-off values between normal and pathologic states. These issues derive from methodological differences in design and technology, measurement errors and heterogeneity in the sample population among research papers (43, 44).

Although 90% of peripheral nerve entrapments involve the median nerve at the carpal tunnel, other osteofibrous sites of compression are encountered in clinical practice. In ulnar nerve compressive neuropathy at the elbow, for example, the second most common entrapment neuropathy, the cut-off threshold was between 7.5 to 10 mm<sup>2</sup> (45-49) when measured proximal to the medial epicondyle. Some authors use a CSA at its site of maximal enlargement in excess of 9mm<sup>2</sup> or a ratio greater than 2.8 when compared to a proximal CSA to diagnose entrapment.

#### *Carpal tunnel syndrome*

In carpal tunnel syndrome, a number of studies have examined the parameters of the median nerve that are most useful for the diagnosis. It has been shown that the nerve cross-sectional area (CSA) is significantly greater in patients with carpal tunnel syndrome than in controls (50-53). Based on the available literature, the most commonly accepted CSA threshold to diagnose carpal tun-



**Fig. 9.** Dissection of median nerve shows a bifid median nerve at the entry to the carpal tunnel due to a high or proximal division (yellow markers).

nel syndrome is  $\geq 10\text{mm}^2$  at the pisiform level or the tunnel inlet (44). Some authors suggest that a CSA of the median nerve  $< 8\text{mm}^2$  rules out compression of the carpal tunnel, and  $> 14\text{mm}^2$  rules it in (54). Other authors have suggested that a CSA  $< 6\text{mm}^2$  excludes carpal tunnel syndrome, whereas a value  $> 12\text{mm}^2$  indicates this condition (55). For values falling between this range, they suggest using the difference between CSA at the point of maximum nerve enlargement, and the CSA over the proximal aspect of the pronator quadratus in the forearm ( $\Delta\text{CSA}$ ). Regarding this latter measurement, a difference  $> 2\text{mm}^2$  proved to have 92.5% sensitivity, 96.4% specificity and 93.9% accuracy (56) for the diagnosis. In the presence of a bifid median nerve (*i.e.* proximal median nerve separation), the same method can be used by summing the CSAs of the “radial” and “ulnar” branches of the nerve at the two levels of measurement (57) (Fig. 9).

Other authors proposed the level of the distal wrist crease and 12cm proximally in the forearm for CSA measurement (58). Using this system, an upper limit of normal of the wrist-to-forearm ratio of 1.4 had 100% sensitivity for detecting carpal tunnel syndrome with no false positives in the control group

(58). Differing from the calculation of the CSA at the point of maximum nerve swelling, patient’s weight, body mass index, height and gender do not seem to affect the accuracy of wrist-to-forearm measurements (59). In a more recent study, a correlation between  $\Delta\text{CSA}$  and severity of carpal tunnel syndrome was found with a  $\Delta$  value  $> 6\text{mm}^2$  compatible with moderate severity and  $> 9\text{mm}^2$  with severe disease (60).

The use of CSA as a predictive indicator of clinical outcome after carpal tunnel release remains controversial with conflicting evidence (61-63). Initial experience with US elastography showed that the median nerve is stiffer in patients with carpal tunnel syndrome compared with healthy controls (64, 65).

In carpal tunnel syndrome, intraneural hyperaemia seems to correlate with disease severity and to be a good predictor of median nerve entrapment (35). In longstanding compression, irreversible intraneural fibrosis may occur. In contrast to early disease, nerves with fibrotic changes tend to remain swollen after decompressive surgery and to show poor functional improvement (61).

#### *Traumatic injuries*

The main pathologies involved in nerve trauma include penetrating wounds,

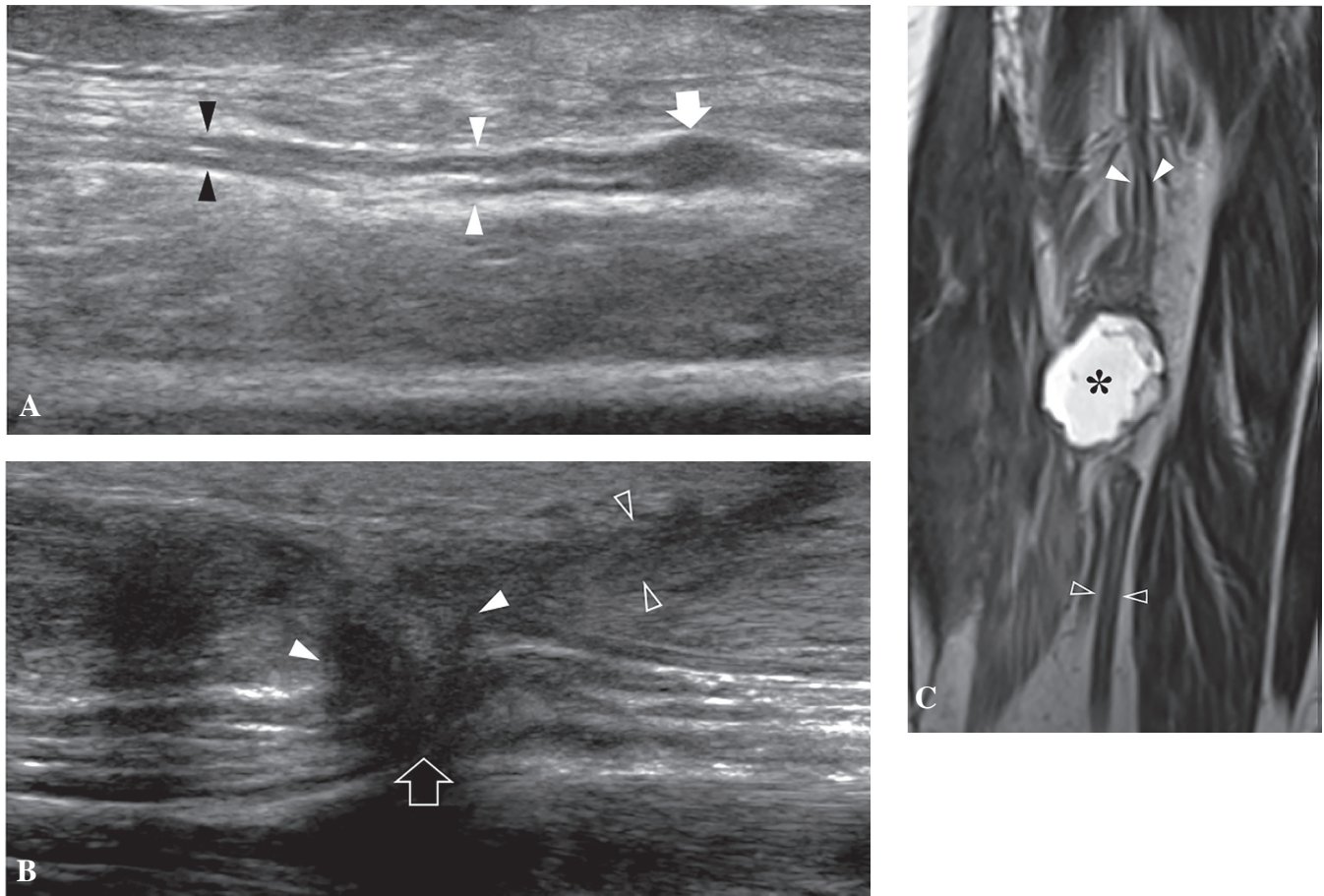


**Fig. 10.** Nerve injuries. Spectrum of imaging appearances in different cases.

**A:** Long-axis 17.5MHz US image of a transected sural nerve following a penetrating glass wound. A small stump neuroma (arrow) is observed in continuity with the proximal nerve end (arrowheads).

**B:** Long-axis 17.5MHz US image of a severed tibial nerve in the distal leg by a penetrating injury. The proximal and distal nerve ends (solid arrowheads) are kept close with each other by scarring tissue without stump retraction. Vacant arrowheads indicate the wound path.

**C:** Coronal T2-weighted MR image over the mid-thigh in a patient with exposed femoral shaft fracture after a traffic accident demonstrates laceration of the sciatic nerve with a haematoma (asterisk) filling the gap between the proximal (white arrowheads) and distal (distal arrowheads) nerve ends.

stretching and contusion injuries. In penetrating injuries, the nerve may be completely severed or there may be a selective injury involving some of its fascicles. At the nerve ends, regenerating Schwann cells, disrupted axons, proliferating fibroblasts and new axonal sprouts expanding randomly to fill the gap between the interrupted fascicles, shape a non-neoplastic mass reflecting disorganised repair, the so-called traumatic neuroma (66).

In complete nerve tears, blunted neuromas develop as small oval mass at the opposite edges of the transected nerve (Fig. 10A). Stump (terminal) neuromas appear as oval hypoechoic masses at US and exhibit hyperintense signal on fluid-sensitive sequences at MR imaging. Most neuromas have well-defined margins but their borders may be poorly

defined when they are attached to scarring tissue at the wound site (67) (Fig. 10B, C). Identification of terminal neuromas may help the diagnosis, especially if the nerve is very small (68). In partial nerve tears, US can estimate the percentage of injured and preserved fascicles using short-axis planes. In these cases, a spindle hypoechoic neuroma may develop from the injured fascicles possibly extending to the whole nerve bundle. US and MR imaging are often unable to assess the status of the fascicles within the neuroma or predict functional outcome and recovery time. In this clinical setting, the main role of imaging is to provide information about the status of the injured nerve and especially in deciding whether an early surgical treatment should be instituted. This is particularly true for minor nerve

lesions or in cases of nerve impingement by fracture fragments, metallic hardware or fibrous encasement.

US has a high negative predictive value in excluding structural nerve damage. Before surgery, careful attention should be placed in measuring the gap between the nerve ends. For this measurement, the examiner should be aware that the neuroma needs to be excised at surgical repair. Therefore, the measurement should be performed not only as the end-to-end distance but also adding the neuromas length to the actual gap length, starting measurement at the base of neuroma where the fascicular echotexture is preserved.

Nerve stretching trauma typically occur following sprain or strain injuries. In complete nerve laceration, US reveals discontinuity of the nerve bundle and its

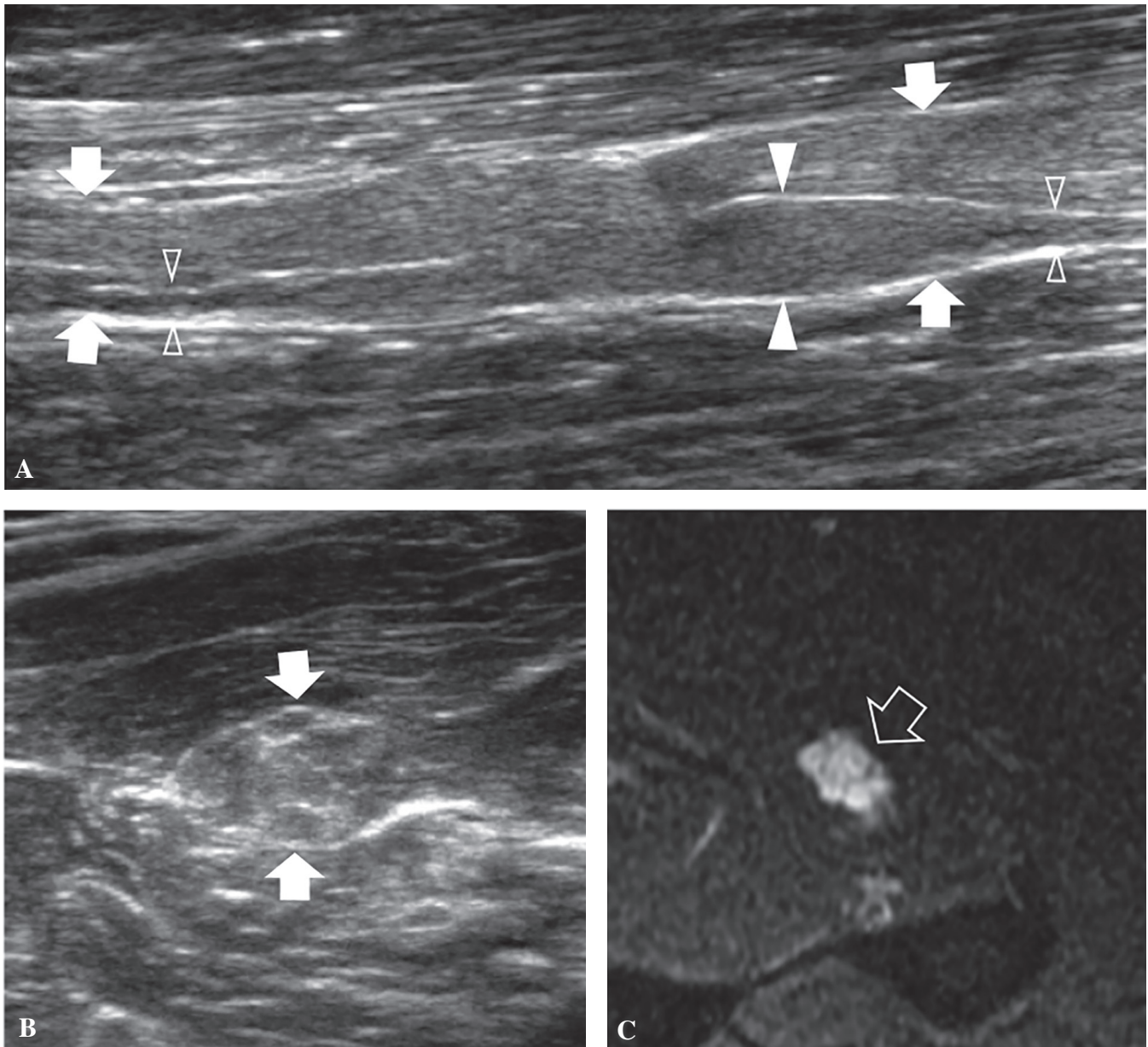


**Fig. 11.** Chronic inflammatory demyelinating polyneuropathy. **A:** Long-axis and **(B)** short-axis 12-5MHz US images of the median nerve (arrows) at the middle forearm shows hyperechoic fascicles characterised by alternating thinned (void arrowheads) and thicker (white arrowheads) segments. **C:** Correlative axial fat-suppressed T2-weighted MR image reveals variable fascicular size and hyperintense signal reflecting oedema and inflammatory infiltrates.

fascicles and a wavy course of the retracted nerve ends (69). In the acute setting, US has advantages over MR imaging in defining the exact position of the nerve ends because oedematous changes, haemorrhage and disrupted tissues at the site of injury may lead to high intensity signal in the nerve surroundings on fluid-sensitive sequences, thus impairing detection of the nerve ends. In the absence of laceration, a fusiform hyperechoic swelling with loss of the fascicular echotexture may develop reflecting a

spindle neuroma with fibrosis internal to a non-disrupted nerve trunk (70). Nerve stretching injuries commonly occur at the brachial plexus level following traffic accidents (71). Stretching injuries may also occur where nerves pierce fascial planes. In case of minor stretching trauma, imaging may be negative. Symptoms include burning in the territory of nerve distribution and some numbness, but these symptoms self-limited and totally reversible. Contusion trauma most often occurs at the

points at which nerves run closely apposed to bony surfaces and are, therefore, vulnerable to external pressure. Most injuries are readily reversible and there is no need for imaging. In severe cases, nerve contusion leads to development of a segmental fusiform thickening of the nerve at the site of trauma. At certain sites (*e.g.* ulnar nerve instability at the epitrochlear groove), the outer epineurium may appear thickened as a result of fibrotic changes, a condition which is also known as friction neuritis.

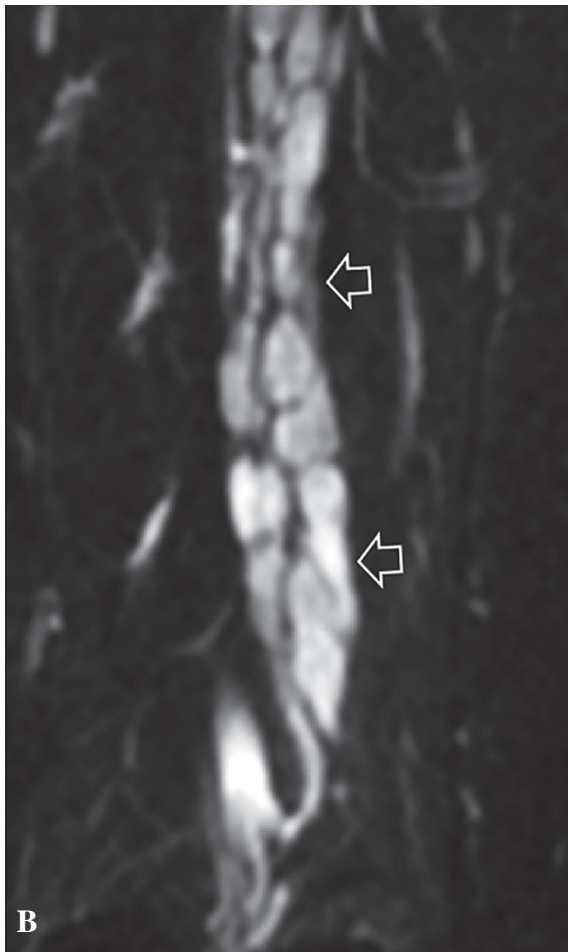
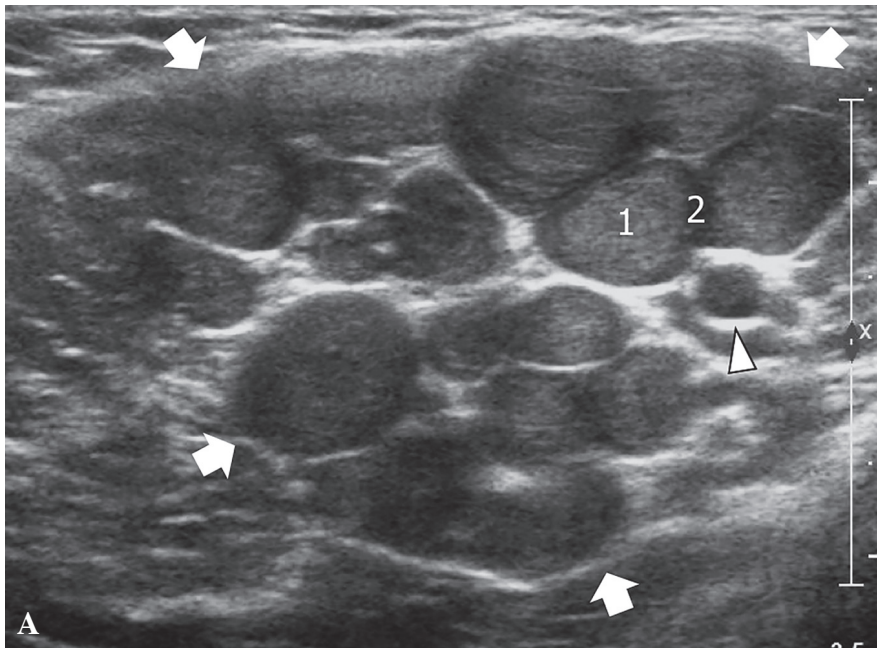


**Fig. 12.** Neurofibromatosis. **A:** Short-axis 12.5-MHz US image of the bicipital sulcus with correlative **(B)** sagittal MR neurography in a patient with type-1 neurofibromatosis. Multiple neurofibromas are found arising from the fascicles of the median nerve (arrows) that looks abnormally enlarged. Note the size of the brachial artery (arrowhead) for comparison. In many lesions, the “target sign” consisting of an extended hyperechoic centre (1) surrounded by a smaller hypoechoic halo (2) is appreciated.

### Polyneuropathies

The term “polyneuropathies” encompasses a clinically heterogeneous group of inherited and immune-mediated disorders of the peripheral nervous system.

In Charcot-Marie-Tooth disease, a marked generalised nerve enlargement characterises the autosomal dominant type, 1A (72). US reveals markedly enlarged nerves with preserved fascicular

pattern (73, 74). Approximately 3-3.5-fold enlargement of the nerve CSA has been observed as compared to controls in both median and ulnar nerves (73). No correlation was found between nerve or fascicle size and conduction velocities (73).

US can aid in classifying the neuropathy as demyelinating or axonal when electrophysiological studies are inconclusive. It may also be useful in patients with unrecognised disease and non-specific symptoms.

In the hereditary neuropathy with liability to pressure palsies (HNPP), US can help the diagnosis when unexpected focal CSA abnormalities are recognised along the nerve course, external to common entrapment sites. This may be relevant for identifying the disease when family history is negative and genetic tests are not available (75). When nerve enlargements occur within osteofibrous tunnels, the increased nerve CSA may mimic an entrapment neuropathy (76). In these instances, HNPP may go unnoticed.

Immune-mediated (dysimmune) polyneuropathies include Guillain-Barré syndrome, chronic inflammatory demyelinating polyradiculoneuropathy (CIDP) and multifocal motor neuropathy (MMN). Because these disorders respond to appropriate therapy, their early recognition and treatment prior to the onset of axonal loss is critical to improve the patient outcomes. Unfortunately, an early diagnosis is not straightforward based on clinical findings and electrophysiological testing, and the disorder often remains unrecognised (77, 78). Unfortunately, nerve imaging appears unlikely to be useful for early diagnosis of Guillain-Barré syndrome.

In contrast to Guillain-Barré syndrome, US can contribute to identify nerve abnormalities in chronic inflammatory demyelinating polyneuropathy (CIDP). In this disorder, focal nerve swelling at the site of conduction blocks can be identified with US and MR imaging (74, 79). The fascicles may appear individually swollen with alternating thick and thin segments (80, 81) (Fig. 11A, B). An inverse correlation between CSA and nerve conduction velocity has been observed (74). The thickened segments

may show marked hyperintensity on fluid-sensitive sequences at MR imaging as a result of intraneural oedema, inflammatory infiltrates and demyelination (82) (Fig. 11C). During treatment, some progression toward normalisation can be seen in the appearance of the affected fascicles before any neurophysiological sign of return to normal becomes apparent (83, 84). Similar to CIDP, US can detect multifocal nerve swellings in multifocal motor neuropathy (85).

#### Nerve tumours

Benign peripheral nerve sheath tumours are derived from the Schwann stem cell and include schwannoma (also called neurinoma or neurilemmoma) and neurofibroma (86). The US diagnosis of these tumours basically relies on detection of a soft-tissue mass in continuity with a nerve at its proximal and distal poles (87, 88) (Fig. 7A). This feature is diagnostic but it may not be manifest in cases of tumours arising from too small and distal nerve branches. In this instance, the appearance of nerve tumours is non-specific and cannot be distinguished from other soft-tissue masses.

A rim of fat (the fat-split sign) suggesting an origin of the mass from the intermuscular space or about a neurovascular bundle is another valuable finding (Fig. 7A). Schwannomas typically appear as eccentrically placed globoid masses (88, 89). They arise from an individual fascicle which remains in-axis with the mass, whereas the spared fascicles are splayed about the neoplasm. Large masses may contain calcified foci, fluid-filled areas (cystic schwannomas) and internal degenerative changes with calcifications (ancient schwannomas). Neurofibromas are intimately associated with the parent nerve and may exhibit a “target sign” consisting of a hyperechoic fibrous centre surrounded by a peripheral hypoechoic rim of myxomatous tissue (90). Three types of neurofibromas have been described on histopathology: localised, diffuse and plexiform. The localised variety represents approximately 90% of these lesions (86, 89). Diffuse neurofibromas present as a plaque-like elevation of

the skin with regional thickening of the subcutaneous tissue. All three types of neurofibromas can be associated with type-1 neurofibromatosis. Plexiform neurofibromas are pathognomonic for this entity, usually involving a long nerve segment and its branches with tortuous expansion, and their gross appearance has been described as a “bag of worms” (86) (Fig. 12).

Malignant transformation in neurofibromatosis has been reported to occur from 2% to 29% of cases (89). Malignant peripheral nerve sheath tumours tend to be larger than benign forms and may exhibit indistinct margins, peripheral enhancement pattern, intratumour cystic areas and perilesional oedema as a result of infiltrative growth (91, 92).

#### Conclusions

US and MR imaging have had a profound impact on the understanding, diagnosis and treatment of disorders of the peripheral nervous system which will continue to expand as our knowledge of these fascinating structures continues to grow. Many of these disorders are the result of systemic diseases within the realm of rheumatic practice. As rheumatologists continue in their admirable pursuit to utilise and improve their proficiency with these imaging modalities, a deep understanding of the PNS is essential.

#### References

1. SACHIN PALVE S, BASHKAR PALVE S: Impact of aging on nerve conduction velocities and late responses in healthy Individuals. *J Neurosci Rural Pract* 2018; 9: 112-6.
2. TONG HC, WERNER RA, FRANZBLAU A: Effect of aging on sensory nerve conduction study parameters. *Muscle Nerve* 2004; 29: 716-20.
3. HUANG CR, CHANG WN, CHANG HW *et al.*: Effects of age, gender, height, and weight on late responses and nerve conduction study parameters. *Acta Neurol Taiwan* 2009; 18: 242-9.
4. BROWN JM, YABLON CM, MORAG Y *et al.*: US of the peripheral nerves of the upper extremity: a landmark approach. *Radiographics* 2016; 36: 452-63.
5. YABLON CM, HAMMER MR, MORAG Y *et al.*: US of the peripheral nerves of the lower extremity: a landmark approach. *Radiographics* 2016; 36: 464-78.
6. TAGLIAFICO A, CADONI A, FISCI E *et al.*: Reliability of side-to-side ultrasound cross-sectional area measurements of lower extremity nerves in healthy subjects. *Muscle Nerve* 2012; 46: 717-22.
7. TAGLIAFICO A, MARTINOLI C: Reliability of side-to-side sonographic cross-sectional area measurements of upper extremity nerves in healthy volunteers. *J Ultrasound Med* 2013; 32: 457-62.
8. PIÑA OVIEDO S, ORTIZ HIDALGO C: The normal and neoplastic perineurium: a review. *Adv Anat Pathol* 2008; 15: 147-64.
9. PLANITZER U, STEINKE H, MEIXENSBERGER J *et al.*: Median nerve fascicular anatomy as a basis for distal nerve prosthesis. *Annals Anat* 2014; 196: 144-9.
10. STEWART JD: Peripheral nerve fascicles: anatomy and clinical relevance. *Muscle Nerve* 2003; 28: 525-41.
11. BIGNOTTI B, TAGLIAFICO A, MARTINOLI C: Ultrasonography of peripheral nerves: anatomy and pathology. *Ultrasound Clin* 2014; 9: 525-36.
12. TAGLIAFICO A: Peripheral nerve imaging: not only cross-sectional area. *World J Radiol* 2016; 8: 726-8.
13. SILVESTRI E, MARTINOLI C, DERCHI LE *et al.*: Echotexture of peripheral nerves: correlation between US and histologic findings and criteria to differentiate tendons *Radiology* 1995; 197: 291-6.
14. GHASEMI-ESFE AR, KHALILZADEH O, VAZIRI-BOZORG SM *et al.*: Color and power Doppler US for diagnosing carpal tunnel syndrome and determining its severity. A Quantitative Image Processing Method. *Radiology* 2011; 261: 499-506.
15. CHOI SJ, AHN JH, RYU DS *et al.*: Ultrasonography for nerve compression syndromes of the upper extremity. *Ultrasonography* 2015; 34: 275-91.
16. KIM S, CHOI JY, HUH YM *et al.*: Role of magnetic resonance imaging in entrapment and compressive neuropathy - what, where, and how to see the peripheral nerves on the musculoskeletal magnetic resonance image: part 1. Overview and lower extremity. *Eur Radiol* 2007; 17: 139-49.
17. CHAPPELL KE, ROBSON MD, STONEBRIDGE-FOSTER A *et al.*: Magic angle effects in MR neurography. *AJNR Am J Neuroradiol* 2004; 25: 431-40.
18. MARTINOLI C, DERCHI LE, BERTOLOTTO M *et al.*: US and MR imaging of peripheral nerves in leprosy. *Skeletal Radiol* 2000; 29: 142-50.
19. FILLER AG, KLIOT M, HOWE FA *et al.*: Application of magnetic resonance neurography in the evaluation of patients with peripheral nerve pathology. *J Neurosurg* 1996; 85: 299-309.
20. FILLER AG, HOWE FA, HAYES CE *et al.*: Magnetic resonance neurography. *Lancet* 1993; 341: 659-61.
21. FILLER AG, MARAVILLA KR, TSURUDA JS: MR neurography and muscle MR imaging for image diagnosis of disorders affecting the peripheral nerves and musculature. *Neurol Clin* 2004; 22: 643-82.
22. CHHABRA A, CARRINO J: Current MR neurography techniques and whole-body MR neurography. *Semin Musculoskelet Radiol* 2015; 19: 79-85.
23. MADHURANTHAKAM AJ, LENKINSKI RE: Technical advancements in MR neurography. *Semin Musculoskelet Radiol* 2015; 19: 86-93.

24. HOWE FA, FILLER AG, BELL BA, GRIFFITHS JR: Magnetic resonance neurography. *Magn Reson Med* 1992; 28: 328-38.
25. MOORE KR, TSURUDA JS, DAILEY AT: The value of MR neurography for evaluating extraspinal neuropathic leg pain: a pictorial essay. *AJNR Am J Neuroradiol* 2001; 22: 786-94.
26. HILTUNEN J, SUORTTI T, ARVELA S *et al.*: Diffusion tensor imaging and tractography of distal peripheral nerves at 3 T. *Clin Neurophysiol* 2005; 116: 2315-23.
27. SKORPIL M, KARLSSON M, NORDELL A: Peripheral nerve diffusion tensor imaging. *Magn Reson Imaging* 2004; 22: 743-5.
28. CHHABRA A, MADHURANTHAKAM AJ, ANDREISEK G: Magnetic resonance neurography: current perspectives and literature review. *Eur Radiol* 2018; 28: 698-707.
29. TAKAGI T, NAKAMURA M, YAMADAM *et al.*: Visualization of peripheral nerve degeneration and regeneration: monitoring with diffusion tensor tractography. *NeuroImage* 2009; 44: 884-92.
30. KABAKCIN, GURSES B, FIRAT Z *et al.*: Diffusion tensor imaging and tractography of median nerve: normative diffusion values. *AJR Am J Roentgenol* 2007; 189: 923-27.
31. KAMATH S, VENKATANARASIMHAN, WALSH MA *et al.*: MRI appearance of muscle denervation. *Skeletal Radiol* 2008; 37: 397-404.
32. HOLL N, ECHANIZ-LAGUNA A, BIERRY G *et al.*: Diffusion-weighted MRI of denervated muscle: a clinical and experimental study. *Skeletal Radiol* 2008; 37: 1111-7.
33. MARTINOLI C, BIANCHI S, GANDOLFO N *et al.*: US of nerve entrapments in osteofibrous tunnels of the upper and lower limbs. *Radiographics* 2000; 20: 199-217.
34. GHASEMI-ESFE AR, KHALILZADEH O, VAZIRI-BOZORG SM *et al.*: Color and power Doppler US for diagnosing carpal tunnel syndrome and determining its severity: a quantitative image processing method. *Radiology* 2011; 261: 499-506.
35. MALLOUHI A, PÜLTZL P, TRIEB T *et al.*: Predictors of carpal tunnel syndrome: accuracy of gray-scale and power Doppler sonography. *Am J Roentgenol* 2006; 186: 1240-5.
36. KWEE RM, CHHABRA A, WANG KC *et al.*: Accuracy of MRI in diagnosing peripheral nerve disease: a systematic review of the literature. *AJR Am J Roentgenol* 2014; 203: 1303-9.
37. CHALIAN M, BEHZADI AH, SHORES JT *et al.*: High-resolution magnetic resonance neurography in upper extremity neuropathy. *Neuroimaging Clin N Am* 2014; 24: 109-25.
38. SPRATT JD, STANLEY AJ, GRAINGER AJ *et al.*: The role of diagnostic radiology in compressive and entrapment neuropathies. *Eur Radiol* 2002; 12: 2352-64.
39. ANDREISEK G, BURG D, STUDER A *et al.*: Upper extremity peripheral neuropathies: role and impact of MR imaging on patient management. *Eur Radiol* 2008; 18: 1953-61.
40. SUBHAWONG TK, WANG KC, THAWAIT SK *et al.*: High resolution imaging of tunnels by magnetic resonance neurography. *Skeletal Radiol* 2012; 41: 15-31.
41. BASHIR WA, CONNELL DA: Imaging of entrapment and compressive neuropathies. *Semin Musculoskelet Radiol* 2008; 12: 170-82.
42. HOCHMAN MG, ZILBERFARB JL: Nerves in a pinch: imaging of nerve compression syndromes. *Radiol Clin North Am* 2004; 42: 221-45.
43. THOIRS K, WILLIAMS MA, CERT G *et al.*: Ultrasonographic measurements of the ulnar nerve at the elbow. *J Ultrasound Med* 2008; 27: 737-43.
44. MCDONAGH C, ALEXANDER M, KANE D: The role of ultrasound in the diagnosis and management of carpal tunnel syndrome: a new paradigm. *Rheumatology (Oxford)* 2015; 54: 9-19.
45. KIM JH, WON SJ, RHEE WI, PARK HJ, HONG HM: Diagnostic cutoff value for ultrasonography in the ulnar neuropathy at the elbow. *Ann Rehabil Med* 2015; 39: 170-5.
46. WIESLER ER, CHLOROS GD, CARTWRIGHT MS, SHIN HW, WALKER FO: Ultrasound in the diagnosis of ulnar neuropathy at the cubital tunnel. *J Hand Surg Am* 2006; 31: 1088-93.
47. YOON JS, KIM BJ, KIM SJ *et al.*: Ultrasonographic measurements in cubital tunnel syndrome. *Muscle Nerve* 2007; 36: 853-5.
48. GRUBER H, GLODNY B, PEER S: The validity of ultrasonographic assessment in cubital tunnel syndrome: the value of a cubital-to-humeral nerve area ratio (CHR) combined with morphologic features. *Ultrasound Med Biol* 2010; 36: 376-82.
49. YALCIN E, UNLU E, AKYUZ M, KARAAHMET OZ: Ultrasound diagnosis of ulnar neuropathy: comparison of symptomatic and asymptomatic nerve thickness. *J Hand Surg Eur Vol* 2014; 39: 167-71.
50. DUNCAN I, SULLIVAN P, LOMAS F: Sonography in the diagnosis of carpal tunnel syndrome. *AJR Am J Roentgenol* 1999; 173: 681-4.
51. LEE D, VAN HOLSBECK M, JANEVSKI P *et al.*: Diagnosis of carpal tunnel syndrome. Ultrasound vs. electromyography. *Radiol Clin North Am* 1999; 37: 859-72.
52. SEMIK R, ABLCALAF C, PIMENTAL B *et al.*: Ultrasound features of carpal tunnel syndrome: a prospective case control study. *Skeletal Radiol* 2008; 37: 49-53.
53. KIM J, KIM M, KO Y: Correlating ultrasound findings of carpal tunnel syndrome with nerve conduction studies. *Muscle Nerve* 2013; 48: 905-10.
54. CHEN Y, WILLIAMS L, ZAK M *et al.*: Review of ultrasonography in the diagnosis of carpal tunnel syndrome and a proposed scanning protocol. *J Ultrasound Med* 2016; 35: 2311-24.
55. PEETRONIS PA, DERBALI W: Carpal tunnel Syndrome. *Semin Musculoskelet Radiol* 2013; 17: 28-33.
56. KLAUSER AS, HALPERN EJ, DE ZORDO *et al.*: Carpal tunnel syndrome assessment with US: value of additional cross-sectional area measurements of the median nerve in patients versus healthy volunteers. *Radiology* 2009; 250: 171-7.
57. KLAUSER AS, HALPERN EJ, FASCHINGBAUER R *et al.*: Bifid median nerve in carpal tunnel syndrome: assessment with US cross-sectional area measurement. *Radiology* 2011; 259: 808-15.
58. HOBSON-WEBB L, MASSEY J, JUEL V, SANDERS D: The sonographic wrist-to-forearm median nerve area ratio in carpal tunnel syndrome. *Clin Neurophysiol* 2008; 119: 1353-7.
59. WON SJ, KIM BJ, PARK KS *et al.*: Reference values for nerve ultrasonography in the upper extremity. *Muscle Nerve* 2013; 47: 864-71.
60. KLAUSER AS, ABD ELLAH MM, HALPERN EJ *et al.*: Sonographic cross-sectional area measurement in carpal tunnel syndrome patients: can delta and ratio calculations predict severity compared to nerve conduction studies? *Eur Radiol* 2015; 25: 2419-27.
61. MONDELLI M, FILIPPOU G, ARETINI A *et al.*: Ultrasonography before and after surgery in carpal tunnel syndrome and relationship with clinical and electrophysiological findings. A new outcome predictor? *Scand J Rheumatol* 2008; 37: 219-24.
62. BLAND JDP, RUDOLFER SM: Ultrasound imaging of the median nerve as a prognostic factor for carpal tunnel decompression. *Muscle Nerve* 2014; 49: 741-4.
63. MARSCHALL A, FICJIAN A, STRADNER MH *et al.*: The value of median nerve sonography as a predictor for short- and long-term clinical outcomes in patients with carpal tunnel syndrome: a prospective long-term follow-up study. *PLoS One* 2016; 11: e0162288.
64. ORMAN G, OZBEN S, HUSEYINOGLU *et al.*: Ultrasound elastographic evaluation in the diagnosis of carpal tunnel syndrome: initial findings. *Ultrasound Med Biol* 2013; 39: 1184-9.
65. MIYAMOTO H, HALPERN EJ, KASTLUNGER M *et al.*: Carpal tunnel syndrome: diagnosis by means of median nerve elasticity: improved diagnostic accuracy of US with sonoelastography. *Radiology* 2014; 270: 481-6.
66. CHIOU HJ, CHOU YH, CHIOU SY *et al.*: Peripheral nerve lesions: role of high-resolution US. *Radiographics* 2003; 23: E15.
67. BODNER G, BUCHBERGER W, SCHOCKE M *et al.*: Radial nerve palsy associated with humeral shaft fracture: evaluation with US: initial experience. *Radiology* 2001; 219: 811-6.
68. TAGLIAFICO A, PUGLIESE F, BIANCHI S *et al.*: High-resolution sonography of the palmar cutaneous branch of the median nerve. *AJR Am J Roentgenol* 2008; 191: 107-14.
69. PEER S, BODNER G, MAIRER R *et al.*: Examination of postoperative peripheral nerve lesions with high-resolution sonography. *AJR Am J Roentgenol* 2001; 177: 415-9.
70. MARTINOLI C, TAGLIFICIO A, BIANCHI S *et al.*: Nerve abnormalities. *Ultrasound Clin* 2007; 2: 655-67.
71. GRAIF M, MARTINOLI C, ROCKIND S *et al.*: Sonographic evaluation of brachial plexus pathology. *Eur Radiol* 2004; 14: 193-200.
72. SCHENONE A, MANCARDI GL: Molecular basis of inherited neuropathies. *Curr Opin Neurol* 1999; 12: 603-16.
73. MARTINOLI C, SCHENONE A, BIANCHI S *et al.*: Sonography of median nerve in Charcot-Marie-Tooth disease. *AJR Am J Roentgenol* 2002; 178: 1553-6.
74. ZAIDMAN CM, AL-LOZI M, PESTRONK A: Peripheral nerve size in normals and patients with polyneuropathy: an ultrasound study. *Muscle Nerve* 2009; 40: 960-6.
75. LUCCHETTA M, DELLA TORRE C, GRANATA G *et al.*: Sonographic features in hereditary neuropathy with liability to pressure palsies. *Muscle Nerve* 2012; 45: 920-1.
76. HOOPER DR, LAWSON W, SMITH L *et al.*:

- Sonographic features in hereditary neuropathy with liability to pressure palsies. *Muscle Nerve* 2011; 44: 862-7.
77. DE SOUSA EA, CHIN RL, SANDER HW, LATOV N, BRANNAGAN TH 3RD: Demyelinating findings in typical and atypical chronic inflammatory demyelinating polyneuropathy: sensitivity and specificity. *J Clin Neuromuscul Dis* 2009; 10: 163-9.
  78. MAGDA P, LATOV N, BRANNAGAN TH 3RD, WEIMER LH, CHIN RL, SANDER HW: Comparison of electrodiagnostic abnormalities and criteria in a cohort of patients with chronic inflammatory demyelinating polyneuropathy. *Arch Neurol* 2003; 60: 1755-9.
  79. GRANATA G, PAZZAGLIA C, CALANDRO P et al.: Ultrasound visualization of nerve morphological alteration at the site of conduction block. *Muscle Nerve* 2009; 40: 1068-70.
  80. TANIGUCHI N, ITOH K, WANG Y et al.: Sonographic detection of diffuse peripheral nerve hypertrophy in chronic inflammatory demyelinating polyradiculoneuropathy. *J Clin Ultrasound* 2000; 28: 488-91.
  81. MATSUOKA N, KOHRIYAMA T, OCHI K et al.: Detection of cervical nerve root hypertrophy by ultrasonography in chronic inflammatory demyelinating polyradiculoneuropathy. *J Neurol Sci* 2004; 219: 15-21
  82. ISHIKAWA T, ASAKURA K, MIZUTANI Y et al.: MR neurography for the evaluation of CIDP. *Muscle Nerve* 2017; 55: 483-9.
  83. DECARD BF, PHAM M, GRIMM A: Ultrasound and MRI of nerves for monitoring disease activity and treatment effects in chronic dysimmune neuropathies: current concepts and future directions. *Clin Neurophysiol* 2018; 129: 155-67.
  84. ALMEIDA V, MARIOTTI P, VELTRI S et al.: Nerve ultrasound follow-up in a child with Guillain-Barré syndrome. *Muscle Nerve* 2012; 46: 270-5.
  85. MEROLAA, ROSSO M, ROMAGNOLO A, PECI E, COCITO D: Peripheral nerve ultrasonography in chronic inflammatory demyelinating polyradiculoneuropathy and multifocal motor neuropathy: correlation with clinical and neurophysiological data. *Neurol Res Int* 2016; 2016: 9478593.
  86. MURPHEY MD, SMITH WS, SMITH SE, KRANSDORF MJ, TEMPLE HT: Imaging of musculoskeletal neurogenic tumors: radiologic-pathologic correlation. *Radiographics* 1999; 19:1 253-80.
  87. BEGGS I: Sonographic appearances of nerve tumors. *J Clin Ultrasound* 1999; 27: 363-8.
  88. LIN J, MARTELL W: Cross-sectional imaging of peripheral nerve sheath tumors: characteristic signs on CT, MR imaging, and sonography. *AJR Am J Roentgenol* 2001; 176: 75-82.
  89. ABREU E, AUBERT S, WAVREILLE G, GHENOR, CANELLA C, COTTON A: Peripheral tumor and tumor-like neurogenic lesions. *Eur J Radiol* 2013; 82: 38-50.
  90. GRUBER H, GLODNY B, BENDIX N, TZANKOV A, PEER S: High-resolution ultrasound of peripheral neurogenic tumors. *Eur Radiol* 2007; 17: 2880-8.
  91. REYNOLDS DL JR, JACOBSON JA, INAMPUDI P, JAMADAR DA, EBRAHIM FS, HAYES CW: Sonographic characteristics of peripheral nerve sheath tumors. *AJR Am J Roentgenol* 2004; 182: 741-4.
  92. WASA J, NISHIDA Y, TSUKUSHI S et al.: MRI features in the differentiation of malignant peripheral nerve sheath tumors and neurofibromas. *AJR Am J Roentgenol* 2010; 194: 1568-74.